Second moment closure analysis of the backstep flow database

By S. Parneix, D. Laurence[1] AND P. Durbin[2]

A second moment closure computation (SMC) is compared in detail with the direct numerical simulation (DNS) data of Le and Moin for the backstep flow at $Re = 5,000$ in an attempt to understand why the intensity of the backflow and, consequently, the friction coefficient in the recirculation bubble are severely underestimated. The data show that this recirculation bubble is far from being laminar except in the very near wall layer. A novel 'differential *a priori*' procedure was used, in which the full transport equation for one isolated component of the Reynolds stress tensor was solved using DNS data as input. Conclusions are then different from what would have been deduced by comparing a full simulation to a DNS. One cause of discrepancy was traced back to insufficient transfer of energy to the normal stress by pressure strain, but was not cured. A significant finding, confirmed by the DNS data in the core region of a channel flow, is that the coefficient that controls destruction of dissipation, C_{ε_2}, should be decreased by a factor of 2 when production is vanishing. This is also the case in the recirculation bubble, and a new formulation has cured 25% of the backflow discrepancy.

1. Introduction

The flow over a backward-facing step has been probably the most popular separated flow test case of the past 20 years, for which numerous experiments (by Kim, Johnston, Eaton, Vogel, Durst, Driver, etc.) provide data on the effects of geometry, inlet conditions, and Reynolds number. With the improvement of turbulence models and numerical methods, it is now generally possible to recover the reattachment length, but the intensity of the backflow and, as a consequence, the negative peak in skin friction are always underestimated by nearly a factor of 2 when second moment closures (SMC) are used.

The recent DNS database of Le and Moin (1993) at $Re = 5,000$, well corroborated by the experiments of Jovic & Driver (1995) and of Kasagi *et al.* (1995), is analyzed here to understand this severe defect common to all SMC.

2. Full simulation of the backward-facing step

The flow was computed using INS2D, a finite difference code in generalized coordinates written at NASA Ames Research Center. A fine, non-uniform grid of

1 Electricité de France, DER, Lab. Nat. d'Hydraulique, 6 quai Watier, 78400 Chatou, France
2 Stanford University

120 × 120 cells was used to cover the region $x/h = -3$ to 35, $x = 0$ being the location of the sudden expansion and h being the step height. The inlet values for the mean velocities, Reynolds stresses, and dissipation were taken from the DNS database. The elliptic relaxation procedure of Durbin (1993) has been combined with the Speziale, Sarkar, Gatski (SSG) pressure strain model in the 'neutral' formulation as in Laurence *et al.* (1995) (see Appendix).

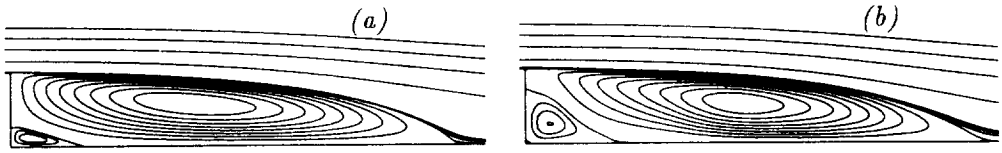

FIGURE 1. Streamlines (a) Second moment closure, (b) DNS

Figure 1 shows the predicted streamlines compared to the DNS data. The reattachment is correct and a secondary bubble is found. However, the size of this corner bubble is much smaller in the simulation than in the data. In fact, if one looks at the predicted friction coefficient compared to the DNS and experimental data (Fig. 2), the intensity of the main recirculation is underpredicted by a factor 1/2 (the slight improvement shown by a dashed curved is discussed further in section 5). The stagnating flow between the two recirculations at $x/h = 2$ is also missed. Since it is believed that the underestimation of the secondary bubble is a consequence of the underestimation of the primary recirculation, we will concentrate in the following on curing the latter discrepancy. Note that the recovery after reattachment is also too slow—this is a problem in virtually all turbulence transport models.

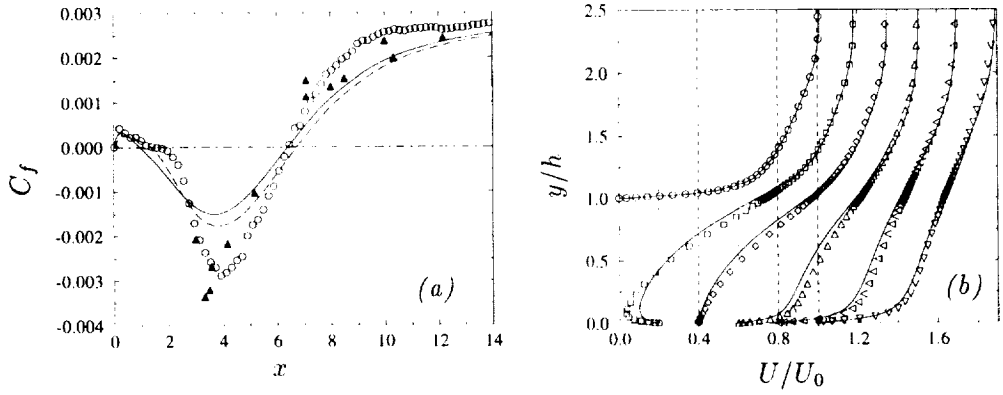

FIGURE 2. (a) Friction coefficient, ○ DNS (Le & Moin), ▲ experiment (Jovic & Driver), —— SMC, ---- modified SMC (cf. section 5), (b) DNS U-profiles at locations $x/h = -3$ (○), 4 (□), 6 (◇), 10 (△), 15 (◁) and 19 (▽), —— : model.

The above observations are believed to reflect what can be expected from any state of the art SMC. In Fig. 2, the mean streamwise velocity U is shown. The center of the recirculation is well predicted, but its intensity is severely underestimated

(see station $x/h = 4$). Since C_f is too weak, this is not due to an overprediction of turbulent mixing in the near wall region, but rather to an underestimation of the entrainment from the shear layer. Since the flow in the upper layer splits at the stagnation point into the recirculation and the downstream flow, this same velocity defect is transported into the recovery region. Le & Moin noted, in good agreement with the Jovic & Driver experiment, that the log profile of the law of the wall was still not recovered at $x/h = 19$; this as a consequence of the low Reynolds number. In the Reynolds-averaged Navier-Stokes (RANS) computation, the recovery at $x/h = 19$ is, however, still slightly underestimated.

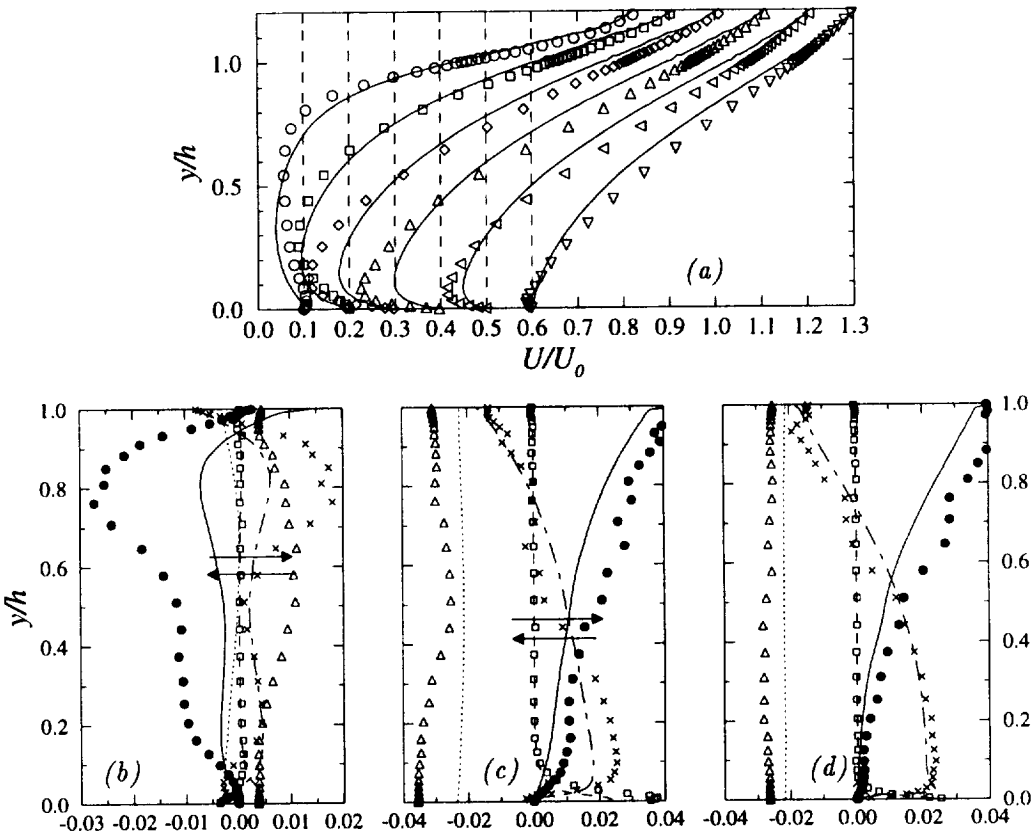

FIGURE 3. (a) Zoom of U in recirculation at locations $x/h = 1$ (○), 2 (□), 3 (◇), 4 (△), 5 (◁) and 6 (▽), ——— : model. (bcd) Budget of U at locations (b) $x/h = 2$ (c) $x/h = 4$ (d) $x/h = 6$, convection (• DNS, ——— SMC) turbulent force (× DNS, — - — SMC), viscous force (□ DNS, - - - - SMC), pressure force (△ DNS, ····· SMC).

Figure 3 focuses on the recirculation and shows the budgets of the U momentum equation. The underestimation of the backflow is most severe at station $x/h = 4$. As expected, the adverse pressure gradient driving the backflow is fairly constant across the whole height and balances the viscous shear stress at the wall; hence, the pressure gradient determines the value of $C_{f_{min}}$. Jovic and Driver (1995) found

that the minimum of C_f follows a 'laminar like' law, $C_{f_{min}} = -0.19 Re_h^{-1/2}$ for Reynolds numbers between 5,000 and 50,000. It is very clear, however, that the recirculation is *not* laminar like, except for the very near wall region below the maximum of the reverse flow.

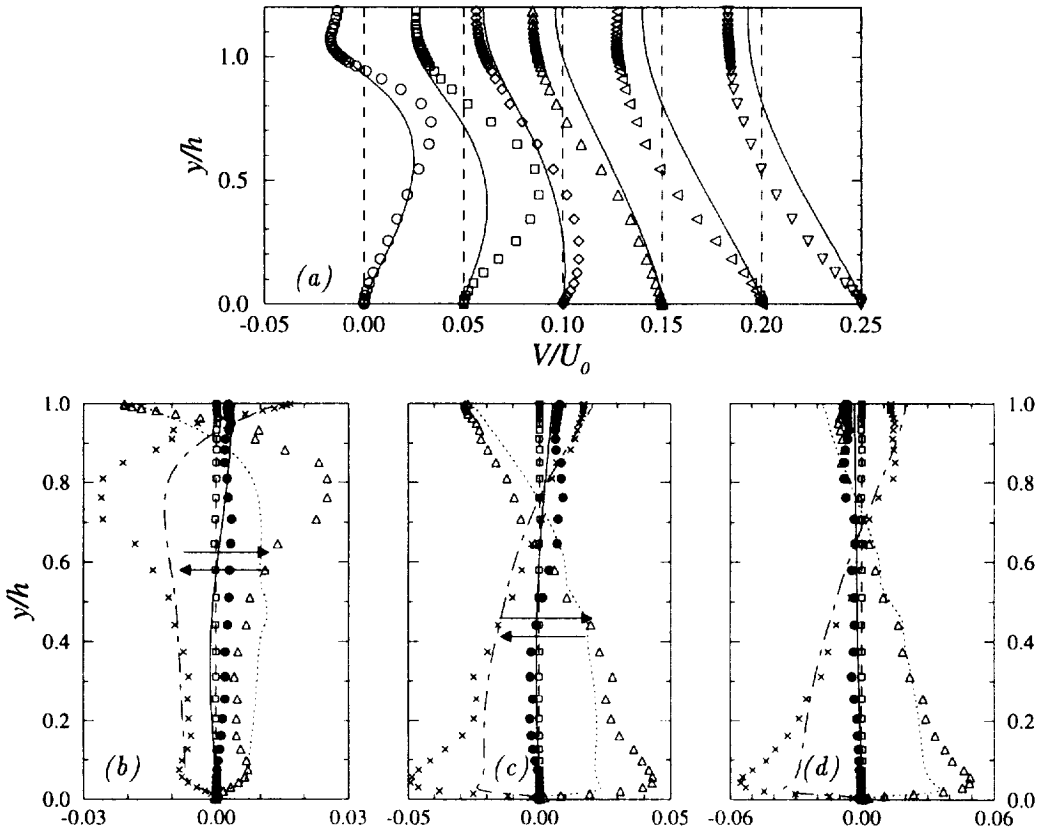

FIGURE 4. (a) Zoom of V in recirculation, legend cf. Fig.3a. (bcd) Budget of V at (b) $x/h = 2$ (c) $x/h = 4$ (d) $x/h = 6$, legend cf. Fig.3bcd.

A possible explanation for the Reynolds number dependence, consistent with the fact that the turbulent Reynolds number remains high in the recirculation bubble, might be as follows. The pressure field is a consequence of the general form of the separated layer (which causes flow expansion and pressure rise). The form of the separated layer is determined by the turbulence. The Reynolds number influence noted by Jovic and Driver (1995) might come from a wider (compared to h) shear layer detaching from the step, causing a stronger adverse pressure gradient at lower values of Re. This view is supported by our observation that RANS computations were more sensitive to model changes in the shear layer than in the recirculating flow. The near-wall, viscous layer of reversed flow results from a balance of the pressure force and the viscous friction, and covers only a few percent of the bubble height—so this cannot lead to 'laminar like' behavior. The turbulent Reynolds

$k^2\varepsilon/\nu$ (i.e., $\approx 10\nu_t/\nu$) in the bubble is in the range 400 - 500 (Fig. 11), similar to its value in the shear layer. Incidently, this makes any low Reynolds 'damping function' ineffective in the main portion of the bubble.

The momentum budget station at $x/h = 2$ shows that entrainment by the turbulent shear stress is underestimated right below the shear layer detaching from the corner. At $x/h = 4$ it was checked that $\overline{uv}$ and VdU/dy are by far the major contributors to the turbulent and convection terms. The shear is weakly opposing the recirculation (a pair of arrows in Figs. 3 and 4 indicates the position of $U = 0$) while advection is driving the recirculation in its upper part. Overall, the model seems only slightly to underestimate this turbulent shear force in the full simulation, even if at this stage the defect is traced to insufficient entrainment at the top part of the recirculation. However, we will see that $\overline{uv}$ itself is in error.

The V component in the shear layer shown in Fig. 4 is severely underestimated. The turbulence force was found to be due almost entirely to $\overline{v^2}$. Again, right near the corner, at $x/h = 2$, the turbulent force is underestimated by about a factor of 2, although not far upstream at $x/h = 0$, the RANS results were in accordance with the DNS data. At $x/h = 4$ and 6 (near reattachment), it is still $\overline{v^2}$ which is driving the flow downward. Advection (inertia or streamline curvature) effects are negligible, showing that a reattaching flow is different from an impinging flow. Fig. 1 shows that the streamlines become smoothly tangent to the wall; some RANS simulations have produced a kink in the streamlines at this reattachment point (Hanjalic, 1996).

3. Differential *a priori* tests

3.1 Reynolds stresses

The Reynolds stresses will now be analyzed from two different sets of computations. The first corresponds to the full simulation and explains the mean velocity budgets shown previously. The second is from a differential *a priori* test and permits an analysis of the true effects of the pressure-strain and transport models. The latter results are obtained by solving the full differential equations of each individual stress $\overline{u_i u_j}$ one by one, while the other stresses and the mean flow are taken directly from the DNS database.

An overall glance at Figs. 5-7 explains why a comparison using only the full simulation may entail erroneous conclusions: the full simulation could lead one to believe that the model has problems in the recirculation bubble, whereas the *a priori* test shows that discrepancies are mainly located in the shear layer.

The $\overline{u^2}$ streamwise fluctuation in the *a priori* test is overestimated in the shear layer, but improved in the recirculation when the correct mean velocity (used in the *a priori* test) enters its production. In both the full and *a priori* simulations, the $\overline{v^2}$ component is seen to be underestimated in the shear layer, and elsewhere at station $x/h = 4$. On the other hand, the shear stress seems to be, on average, correct in the full simulation and overestimated in the *a priori* test. This is because in the former an erroneously small value of $\overline{v^2}$ is entering its production term. The origin of the problem lies in insufficient return to isotropy in the SSG pressure-strain

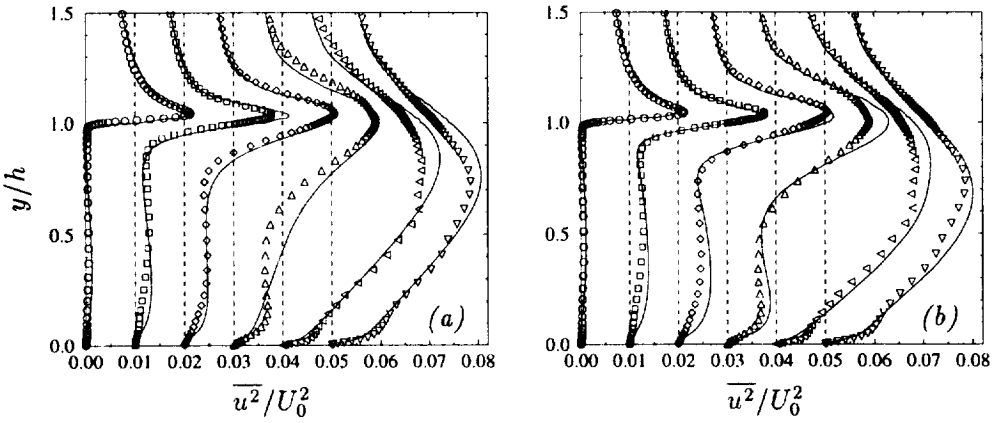

FIGURE 5. $\overline{u^2}$ profiles (a) full computation, (b) *a priori* test, at locations $x/h = 0.1$ (o), 0.5 (□), 1 (◇), 2 (△), 4 (◁) and 6 (▽), ——— : model.

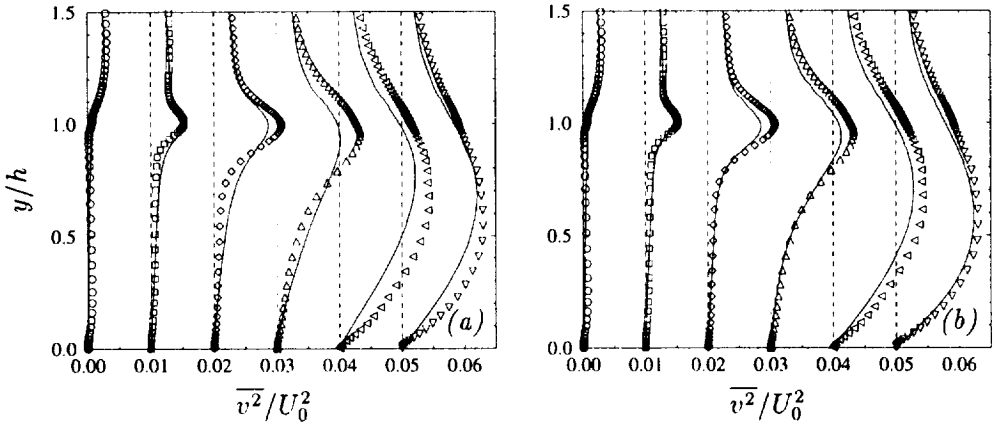

FIGURE 6. $\overline{v^2}$ profiles (a) full computation, (b) *a priori* test, legend cf. Fig.5.

model, which should increase $\overline{v^2}$ and decrease both $\overline{u^2}$ and $\overline{uv}$, but only in the shear layer.

3.2 Budgets

For the analysis of budgets, the DNS data has been processed in the same form as the elliptic relaxation model (see appendix); i.e., some anisotropy effects in the dissipation are lumped with the so-called pressure-strain term.

For the budgets of $\overline{u^2}$ in Fig. 8, the production terms coincide perfectly of course, since the mean velocities and Reynolds stresses other than $\overline{u^2}$, are taken from the DNS. That is the method of this *differential, a priori* test. The model for turbulent transport (Daly-Harlow) performs well, but the pressure gradient-velocity correlation (kf_{12}) is underestimated in the free shear layer.

The budgets of $\overline{v^2}$ (Fig. 9) show here again that in the shear layer the pressure correlation term is underestimated—at $x/h = 2$ by a factor of 2. The pressure term

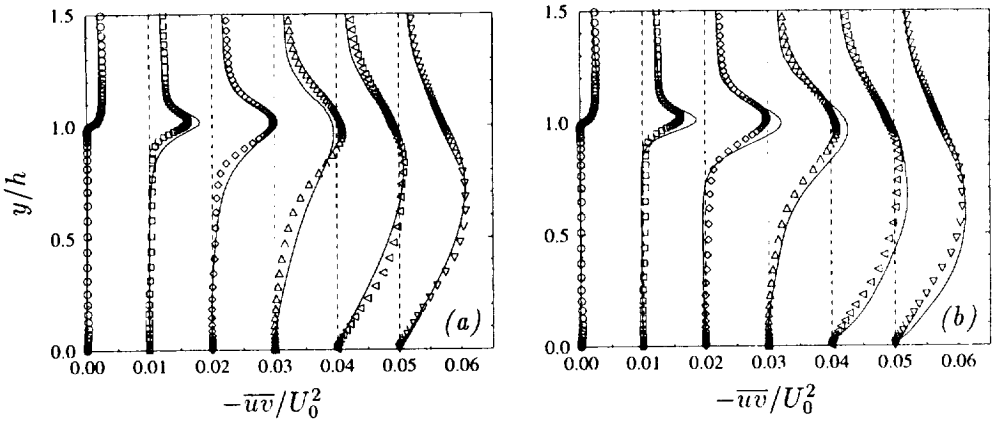

FIGURE 7. $\overline{uv}$ profiles (a) full computation, (b) *a priori* test, legend cf. Fig.5.

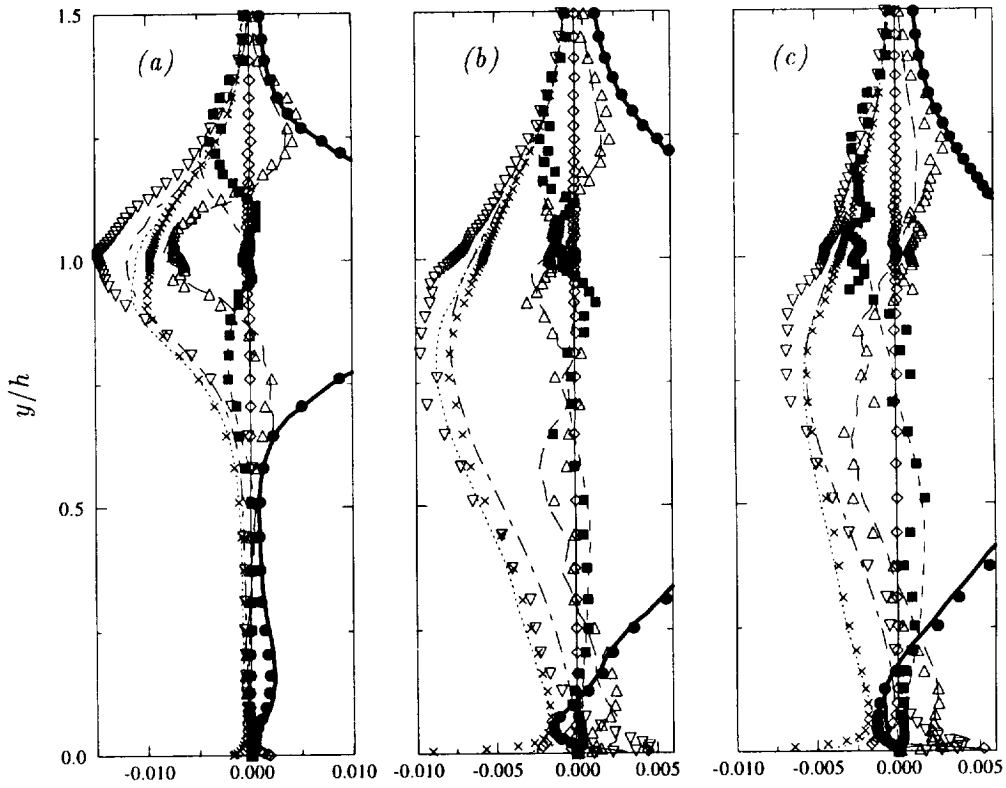

FIGURE 8. *A priori* test: budget of $\overline{u^2}$ at locations (a) $x/h = 2$, (b) $x/h = 4$, (c) $x/h = 6$, production (• DNS, —— SMC), $[-\varepsilon R_{ij}/k]$ (× DNS, ····· SMC), convection (▪ DNS, - - - - SMC), transport (△ triple correlations DNS, — — — SMC), viscous diffusion (◇ DNS, —— SMC), pressure-deformation + dissipation anisotropy effects ($\triangledown[\Pi_{ij}^{vpg} - \varepsilon_{ij} + \varepsilon R_{ij}/k]$ DNS, — - — $[kf_{ij}[$ SMC)

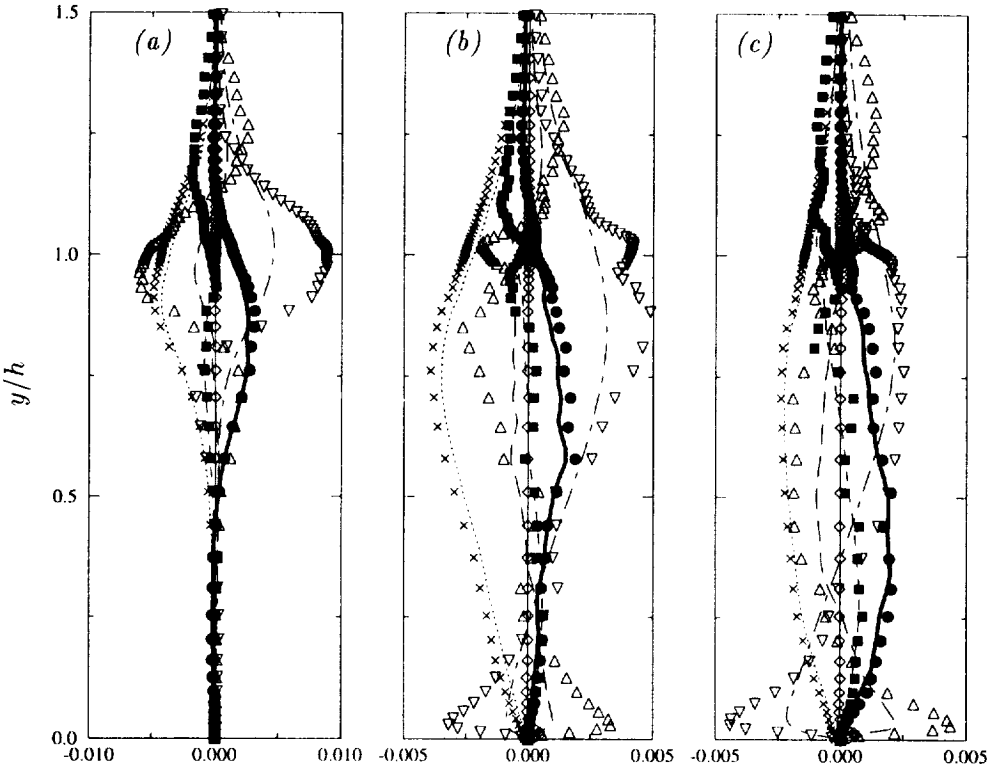

FIGURE 9. *A priori* test: budget of $\overline{v^2}$ at locations (a) $x/h = 2$, (b) $x/h = 4$, (c) $x/h = 6$, legend cf. Fig.8.

includes pressure-transport effects (in the present case countergradient transport effects) which partially balance the turbulent diffusion terms, and which, as a consequence, are also underestimated by the model. Note that the production term is making a significant contribution, and since it is mainly composed of $-\overline{v^2}DV/dy$, underestimations of both $\overline{v^2}$ and V (which is affected by $\overline{v^2}$) self-amplify through this term. Near the wall, turbulent diffusion is generating the wall normal fluctuations, while the wall blocking effect is impeding them; the latter is represented by the elliptic relaxation effect (the homogeneous solution to Eq. 4 of the appendix is actually positive in this area).

The budget of $\overline{uv}$, on the other hand, shows an overestimation of the pressure-correlation, though again this compensates for an underestimation of the turbulent transport. At $x/h = 4$, near the wall, the production term is seen to change sign, but still $\overline{uv}$ remains approximately zero because of the strong transport term. Hence, in the narrow region between the maximum of the backflow and the wall, the mean flow is largely viscous, as seen previously. With increasing Reynolds number, one can expect the ratio of production to transport terms to become larger, and the turbulent shear stress would then decelerate this backflow, leading to a smaller peak in C_f. Because $\overline{uv}$ is countergradient with respect to the velocity gradient,

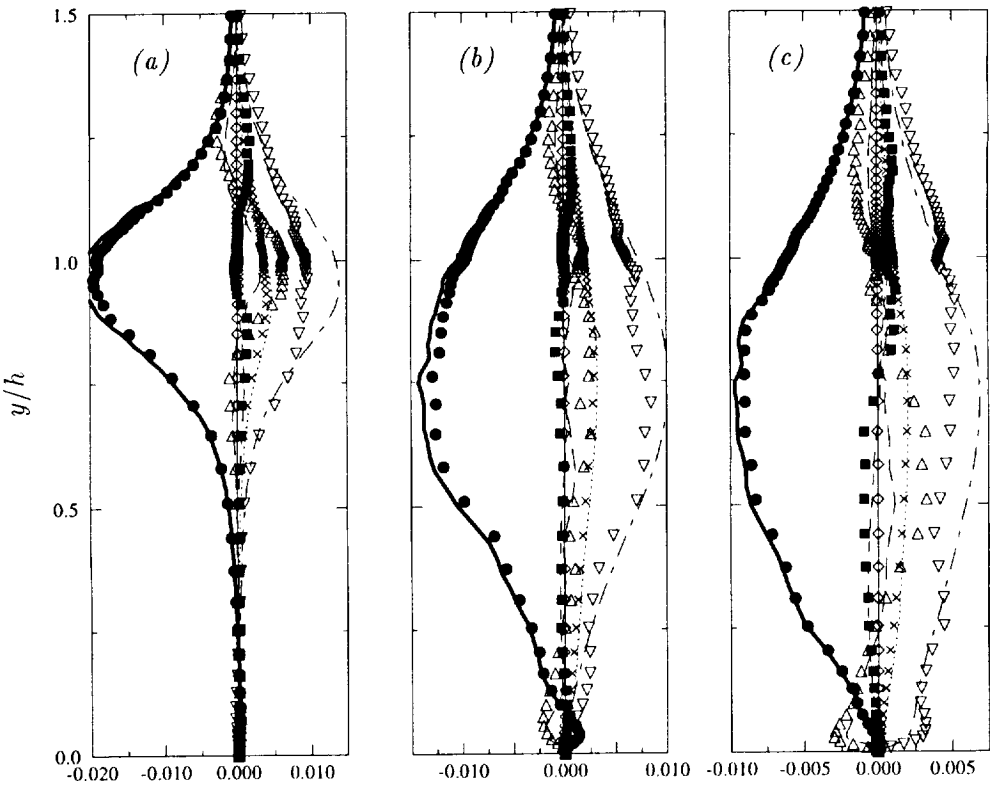

FIGURE 10. *A priori* test: budget of $\overline{uv}$ at locations (a) $x/h = 2$, (b) $x/h = 4$, (c) $x/h = 6$, legend cf. Fig.8.

the production of $\overline{u^2}$ and k becomes negative in this area.

4. Model parameters

Fine tuning of models is often based on functions of the following parameters: anisotropy of the Reynolds stresses, A; turbulent Reynolds number, Re_t; production over dissipation, P/ε (sometimes the non-dimensional rate of strain, Sk/ε is used); and turbulent lengthscale, $k^{3/2}/\varepsilon$. In seeking improvements here, one should look for parameters that exhibit different values from those in simpler shear flows, for which the model should not be changed. The above parameters have been computed from DNS data to see if they are pertinent.

The range of variation of A (Fig. 11) from 0.6 to 0.8 in the recirculation bubble shows no particularity; the Re_t values in the range of 400 to 800 (Fig. 11) is too high to invoke low Reynolds effects; the ratio P/ε (Fig. 12) decreases from 2 to 1.5 in the shear layer, but is seen to be particularly weak in the lower half of the recirculation bubble. This last is a feature that is significantly different from near wall regions of boundary layers and should be considered further. Indeed, even negative production occurs along the wall from the reattachment to $x/h = 4$.

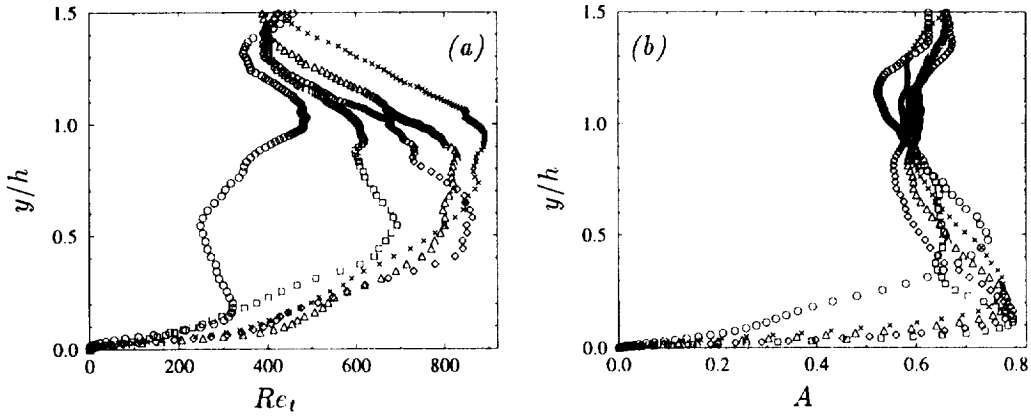

FIGURE 11. DNS profiles (a) Turbulent Reynolds number $Re_t = k^2/(\nu\varepsilon)$, at locations $x/h = 2$ (○), 4 (□), 6 (◇), 8 (△) and 10 (×). (b) Anisotropy $A = 1 - 9/8(A_2 - A_3)$, A_2 and A_3 are the second and third invariants of a_{ij}, legend cf. Fig.11a.

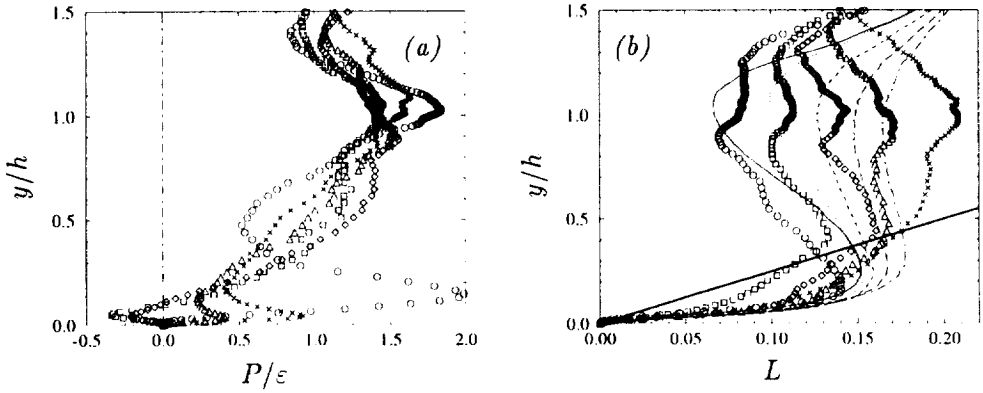

FIGURE 12. DNS profiles (a) Production over dissipation P/ε, legend cf. Fig.11a. (b) Turbulent length scale $L = 0.09^{3/4}k^{3/2}/\varepsilon$, at locations $x/h = 2$ (○ DNS, —— SMC), 4 (□ DNS, ····· SMC), 6 (◇ DNS, - - - - SMC), 8 (△ DNS, — — — SMC) and 10 (× DNS, — - — SMC), κy ——— .

The production of dissipation is usually modeled as proportional to that of k, and negative values might lead here to unphysical effects.

5. Modeling dissipation

Several attempts were made to increase the pressure-strain in the shear layer, but all resulted in a (sometimes dramatic) shortening of the reattachment length, without amplifying the strength of the recirculation. Though the previous analysis indicates that this is a route to pursue, the following only reports some success in improving the dissipation equation.

An *a priori* test of the $k - \varepsilon$ equations was carried out by solving the coupled

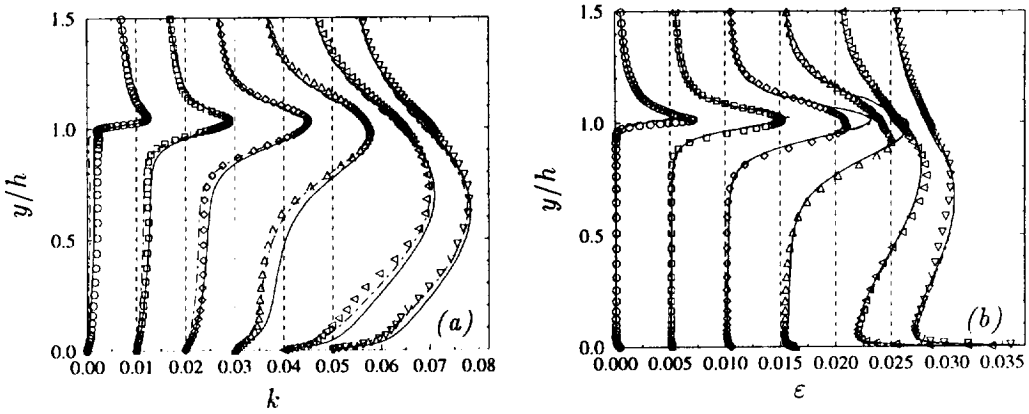

FIGURE 13. *A priori* test: (a) k, (b) ε, at locations $x/h = 0.1$ (○), 0.5 (□), 1 (◇), 2 (△), 4 (◁) and 6 (▽), ——— : model, —·— : modified model (ε equation).

$k - \varepsilon$ system with DNS data for $\overline{u_i u_j}$ and U. Dissipation is, of course, the exact source term for k, but k also has a strong relation to dissipation through the inverse timescale ε/k in front of its source term: this is why the equations were solved as a coupled system.

Figure 13 seems to indicate that k is overestimated and dissipation is correct in the coupled, differential test. In the recirculation bubble the effect of the source term in the ε equation is destruction of ε, since production is low. The 'modification' cited in the figure caption that is detailed below was intended to increase dissipation, but actually it leaves ε unchanged and decreases k, bringing it closer to the DNS. This is because when the source term coefficient in ε equation is decreased, the balance of the dissipation budget is re-established by a decrease of the time-scale, i.e. a decrease of k/ε, that occurs by k decreasing with little change of ε.

Tuning of the dissipation equation has been a popular game for the past two decades, so it needs to be shown that the present modification should not deteriorate predictions in other flows, and what the rationale is behind it.

Various procedures have been developed to enhance dissipation. In near wall flows below $y^+ = 10$, an extra viscous production term is usually included in low Re models. However, it is ineffective here because of the relatively high value of Re_t. Another dissipation enhancement is the 'Yap correction' (Launder 1989), which consists in a positive source term in the dissipation equation that is activated whenever the turbulent lengthscale L is larger than the mixing length κy. Though rather *ad hoc*, this 'Yap correction' has been particularly effective for backstep or sudden expansion flows (Hanjalic 1996), and shows that something peculiar is happening to the dissipation that is still not understood. Indeed Fig. 12 shows that L is overestimated in the recirculation bubble near the wall. Although the Yap correction goes in the right direction, there is no justification for forcing L to be smaller than κy since the DNS data shows it to be considerably larger than this.

Another way to increase the production of ε in the near-wall region is to use the non-dimensionalized parameter P/ε (Durbin 1993). This proved effective for

channel and boundary layer flow, but showed unfortunately high levels of numerical instability in more complex flows. Moreover, this does not suffice in the backflow region since P/ε is fairly small. Durbin and Laurence (1996) recently proposed to replace this unstable term by a ratio of k and $\overline{v^2}$ in the $k-\varepsilon-\overline{v^2}$ model: $C_{\varepsilon_1}(1+a_1\sqrt{k/\overline{v^2}})$ with $a_1 = 1/30$. In this study, we have generalized this idea in the full SMC by introducing the following: $C_{\varepsilon_1}(1+a_1\sqrt{P_{k-\varepsilon}/|P_{SMC}|})$ with $a_1 = 0.035$. $P_{k-\varepsilon} = 0.09kTS_{ij}S_{ji}$ and $P_{SMC} = \overline{u_iu_j}S_{ij}$ are respectively the $k-\varepsilon$ formula for production and the exact Reynolds-stress production. This correction has been found to have similar effects to P/ε in the near-wall region of channel flow, without any numerical instabilities in more complex situations. It does not cure the underestimation of the backflow in the present case; of course, that was not its intent.

Very little data is available concerning the dissipation equation budget aside from the channel flow DNS at CTR. From that data, the following adjustment to destruction of dissipation (which we called 'modified model') was devised: $C_{\varepsilon_2} = 1.83 * f(I_\varepsilon)$ with $I_\varepsilon = (P_\varepsilon + D_\varepsilon)/2D_\varepsilon$. This measures the weight of transport in the budget of ε by using the imbalance of production minus destruction. The function f varies from 1 (for shear flows) to 0.5 when production is zero. In order to preserve numerical stability, we combined this modification with the same adjustment for C_{ε_1} (multiplication by $f(I_\varepsilon)$). The following function f was chosen to avoid non-realistic coefficients: $f(x) = \max(\min(x,1),0.5)$. The result for the backstep as concerns the C_f profile was found to be modest (see Fig. 2), yet it is larger than any results obtained through modifications of the pressure strain model.

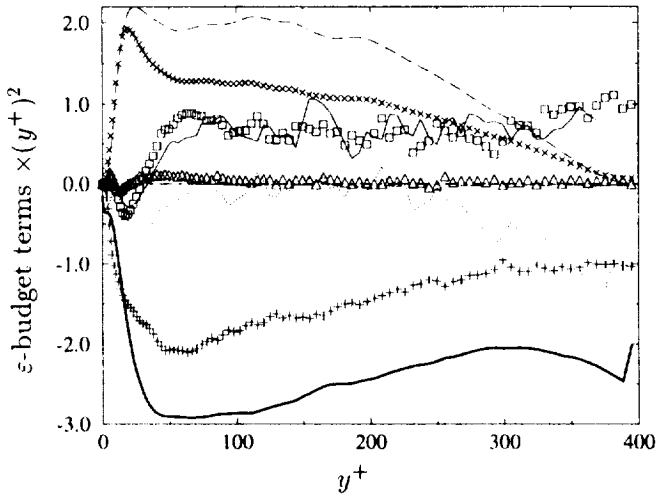

FIGURE 14. Budget of ε for the $Re_\tau = 395$ channel flow, all the terms have been multiplied by $(y^+)^2$, 'rapid part' ($\times$ $[P_1+P_2+P_3]$, – – – modelisation term: $[1.44P_k\varepsilon/k]$) 'slow part' ($+$ $[P_4-\Upsilon]$, ——— modelisation term: $[-1.83\varepsilon^2/k]$), transport (□ DNS, ——— modelisation term), viscous diffusion (△), sum of the modelisation terms (·····).

The idea of re-adjusting C_{ε_2} actually came from the analysis of channel flow at $Re_\tau = 395$, for which the budgets of dissipation are available (Mansour & Kim, private communication). The near wall region has been analyzed in detail by Rodi & Mansour, but what interests us here is the central part of the channel. It is well known to modelers that dissipation is underestimated in the core region, but with little consequence except that the modeled L is continuously increasing instead of leveling off just outside of the log-layer. Since ε decreases as y^{-1} and the terms in its budget are as y^{-2}, all terms in this budget were multiplied by y^2 to produce Fig. 14.

The dissipation budget, as discussed by Mansour, Kim & Moin 1988, or by Mansour & Moin 1993, comprises a viscous transport term, negligible in the core region, a turbulent transport, very well modeled here by gradient diffusion with $\sigma_\varepsilon = 1.3$, and five source terms. It is known on fundamental grounds that these five terms cannot be clearly grouped into production and destruction terms. For the present, the terms involving gradients of velocity are grouped as $P_1 + P_2 + P_3$ and compared to the 'rapid' part of the model, ε/kP_k, while the remaining 'slow' terms are compared to ε^2/k. The DNS values of k and ε are used in the model terms, hence the jagged appearance of the model transport, due to double differentiation of this DNS data. It would seem from Fig. 14 that both constants C_{ε_1} and C_{ε_2} are severely overestimated; but again, the present split is arguable. It is, however, very clear that near the center of the channel, where the rapid terms go to zero, a value of $C_{\varepsilon_2} = 1.83$ is too large by a factor of 2. On the other hand, the transport is accurately modeled with the standard value $\sigma_\varepsilon = 1.3$.

6. Conclusion

A detailed comparison of a SMC computation with the DNS data for the backstep flow at $Re = 5,000$ leads to the following conclusions:

(1) The intensity of the backflow and the friction coefficient in the recirculation bubble are severely underestimated.

(2) The recirculation bubble is far from being pseudo-laminar; an understanding of the problems encountered by SMC should, thus, be of general interest.

(3) The SMC underestimates entrainment out of the recirculating bubble by the detaching shear layer. The mechanism is the following: pressure-strain ϕ_{22} generates normal fluctuations $\overline{v^2}$, which create the transverse mean velocity V; this in turn provides a momentum impulse to the bubble. In the shear layer, ϕ_{22}, $\overline{v^2}$, V are underestimated.

(4) A new *differential a priori* procedure was used, in which the full transport equations are solved one by one.

(5) A modification was proposed to enhance dissipation in, and only in, the recirculation bubble. The new formulation cured 25% of the backflow discrepancy.

(6) The model is supported by a significant finding from the DNS data in the core region of a channel flow: the constant related to destruction of dissipation, C_{ε_2}, should be decreased by a factor of 2 as production vanishes.

REFERENCES

DURBIN, P. 1993 A Reynolds-stress model for near-wall turbulence. *J. Fluid Mech.* **249,** 465-498.

DURBIN, P. A. & LAURENCE, D. 1996 Nonlocal effects in single point closure. *Turbulence Research Associates-96 meeting.* Seoul Korea.

HANJALIC, K. 1996 Some resolved and unresolved issues in modeling non-equilibrium and unsteady turbulent flows. *Engineering Turbulence Modeling and Measurements,* W. Rodi and G. Bergeles Eds., Elsevier Pub. **3,** 3-18.

JOVIC, S, & DRIVER, D. 1995 Reynolds number effect on the skin friction in separated flows behind a backward-facing step. *Experiments in Fluids.* **18.**

KANNICHE, M., LAURENCE, D., & WIZMAN, V. 1995 Combining a second moment closure with elliptic relaxation in rotating turbulent flows. *10th. Symp. on Turbulent Shear Flows, Penn State Pennsylvania.* **20-19.**

KASAGI, N. & MATSUNAGA, A. 1995 Three-dimensional particle-tracking velocimetry measurements of turbulence statistics and energy budget in a backward-facing step flow. *Int. J. Heat and Fluid Flow.* **16,** 477-485.

KO, S. & DURBIN, P. 1994 Separated turbulent flows computed with a near-wall Reynolds stress model. *ASME-FED Summer Meeting.* **196,** 83-92.

LAUNDER, B. E. 1989 Second-moment closure: present ... and future? *Int. J. Heat and Fluid Flow.* **10, N. 4,** 282-300.

LAURENCE, D., DURBIN, P. A. & DEMUREN. A. O. 1995 Modeling near wall effects in second moment closures by elliptic relaxation. *10th. Symp. on Turbulent Shear Flows, Penn State Pennsylvania.* **20-1.**

LE, H., MOIN, P. & KIM, J. 1993 Direct numerical simulation of turbulent flow over a backward-facing step. *Proc. 9th Symp. on Turbulent Shear Flows, Kyoto, Japan.* 13.2.1-13.2.6

MANSOUR, N. N., KIM, J. & MOIN, P. 1988 Reynolds stress and dissipation-rate budgets in a turbulent channel flow. *J. Fluid Mech.* **194,** 15-44.

RODI W. & MANSOUR, N. N. 1993 Low Reynolds number $k - \varepsilon$ modeling with the aid of direct simulation data. *J. Fluid Mech.* **250,** 509-529.

SPEZIALE, C. G., SARKAR, S. & GATSKI, T. B. 1991 Modeling the pressure-strain correlation of turbulence: an invariant dynamical systems approach. *J. Fluid Mech.* **227,** 245-272.

APPENDIX : Elliptic relaxation

The Reynolds stress transport equation is written as:

$$D_t\overline{u_iu_j} = P_{ij} + \varphi_{ij} - \overline{u_iu_j}\frac{\varepsilon}{k} + T_{ij} + \nu\nabla^2\overline{u_iu_j} \tag{1}$$

with

$$\begin{aligned} P_{ij} &= -\overline{u_iu_k}\partial_k U_j - \overline{u_ju_k}\partial_k U_i \\ \varphi_{ij} &= -\overline{u_i\partial_j p} - \overline{u_j\partial_i p} - (\varepsilon_{ij} - \overline{u_iu_j}\frac{\varepsilon}{k}) + \frac{2}{3}\overline{u_k\partial_k p}\delta_{ij} \\ T_{ij} &= -\partial_k(\overline{u_ku_iu_j} + \frac{2}{3}\overline{u_kp}\delta_{ij}) \end{aligned} \tag{2}$$

The term φ_{ij} differs from the usual pressure-strain ϕ_{ij} since it includes a deviatoric dissipation tensor in the form

$$\varphi_{ij} = \phi_{ij} - \left(\varepsilon_{ij} - \overline{u_iu_j}\frac{\varepsilon}{k}\right) \tag{3}$$

The following *neutral* formulation for the elliptic relaxation is now obtained (Durbin and Laurence 1996):

$$\frac{\varphi_{ij}}{k} - L\nabla^2 L\frac{\varphi_{ij}}{k} = \frac{\varphi^h_{ij}}{k} \tag{4}$$

For homogeneous turbulence φ_{ij} ($\equiv kf_{ij}$) in Eq. 4 reduces to φ^h_{ij}, for which any standard redistribution model ϕ^h_{ij} can be used. The SSG rapid model is

$$\phi^h_{ij_{rapid}} = -C_2\mathrm{dev}\,(P_{ij}) - C_3\mathrm{dev}\,(D_{ij}) - C_skS_{ij} \tag{5}$$

The coefficients are:

$$C_2 = \frac{g_4+g_5}{4};\ C_3 = \frac{g_4-g_5}{4};$$
$$C_s = \frac{2}{3}g_4 - g_3 + \frac{g_3^*}{2}\sqrt{A_2}$$

The slow term is of the form

$$\phi^h_{ij_{slow}} = -\left[(C_1+1)a_{ij} + C_1'\mathrm{dev}(a_{ik}a_{kj})\right]\frac{k}{T} \tag{6}$$

$$C_1 + 1 = \frac{1}{2}\left[g_1 + g_1^*\frac{P}{\varepsilon}\right],\ C_1' = -\frac{g_2}{4}$$

The dissipation equation is

$$D_t\varepsilon = \frac{C_{\varepsilon_1}'P - C_{\varepsilon_2}\varepsilon}{T} + \partial_k\left((\nu + \frac{C_\mu\overline{u_ku_l}T}{\sigma_\varepsilon})\partial_l\varepsilon\right) \tag{7}$$

The time scale, T, is defined as:

$$T = \sqrt{\frac{k^2}{\varepsilon^2} + 36\frac{\nu}{\varepsilon}} \tag{8}$$

The length scale L appearing in Eq. 4 also is prevented from going to zero at the wall by using the Kolmogorov scale as a lower bound:

$$L = C_L \sqrt{\frac{k^3}{\varepsilon^2} + C_\eta^2 \frac{\nu^{3/2}}{\varepsilon^{1/2}}} \tag{9}$$

Lastly, the Daly-Harlow expression for the turbulent diffusion is used:

$$T_{ij} = \partial_l \left(C_\mu \overline{u_l u}_m \, T \partial_m \overline{u_i u}_j \right) \tag{10}$$

The constants used in this report are:

$$C_\mu = 0.2, \sigma_\varepsilon = 1.5, C_L = 0.1, C_\eta = 200,$$

$$C_{\varepsilon_1} = 1.44, C_{\varepsilon_2} = 1.83$$

Also

$$\begin{aligned} a_{ij} &= \mathrm{dev}(\overline{u_i u}_j)/k, \; A_2 = a_{ij} a_{ij}, \\ A_3 &= a_{ij} a_{jk} a_{ki}, \; A = 1 - 9(A_2 - A_3)/8 \end{aligned} \tag{11}$$

was used in the text.